Journal of Contemporary Applied Mathematics
V. 17, *No 1*, *2027*, *January-June*
ISSN 2222-5498, E-ISSN 3006-3183
https://doi.org/10.62476/jcam171.5

Mathematical Model of Mechanical Vibrations of a Rectangular Ribbon Loudspeaker

Islam J. Islamov*, Kalin S. Kalinov, Iliyan Y. Iliev

Abstract. This paper presents a comprehensive study of the mechanical vibrations of a ribbon loudspeaker modelled as an elastic body with distributed parameters. Vibrations generated during operation produce spatiotemporal deformations of the ribbon surface, which in turn lead to uneven acoustic radiation and deterioration of sound quality, manifested as resonant peaks, phase distortion, and harmonic distortion.
In this study, the ribbon loudspeaker is modelled as a thin rectangular elastic strip subjected to pre tension and electrodynamic excitation forces. Since the ribbon length significantly exceeds its width and thickness, a one dimensional continuous model of transverse vibrations is employed. Small vibration amplitudes justify the use of linear elasticity theory.
Several lower and higher order vibration modes are analyzed, each characterized by a specific distribution of nodes and antinodes along the ribbon length. The results indicate that high frequency modes have the most detrimental impact on acoustic performance because they produce localized surface deformations and uneven sound pressure distribution.
Numerical analysis of vibration modes is performed using two dimensional and three dimensional modeling in MATLAB® and COMSOL Multiphysics. The simulations allow visualization of natural vibration modes and comparison of numerical results with analytical solutions. To further demonstrate the calculated modes, a video illustrating ribbon deformation dynamics over time was created.
The obtained results confirm the validity of the proposed mathematical model and demonstrate the feasibility of using vibration mode analysis during the design phase of ribbon loudspeakers. The findings can be applied to optimize ribbon geometry, material selection, and tension in order to minimize parasitic resonances and improve sound reproduction quality.

Key Words and Phrases: mathematical model; ribbon loudspeaker; mechanical vibrations; rectangular strip; Rayleigh method; acoustic mass

2010 Mathematics Subject Classifications: AMS classification codes

*Corresponding author.

1. Introduction

Unlike loudspeakers with circular pistons [1–4], ribbon loudspeakers with rectangular strips are more susceptible to structural deformation when excited at their natural frequencies. These deformations produce vibration modes across the ribbon surface, which influence acoustic performance and may lead to structural failure under excessive loading conditions. Understanding critical vibration modes that compromise structural integrity is essential for improving the performance and reliability of ribbon loudspeakers. Identification of these modes enables implementation of protective strategies such as mechanical optimization, damping techniques, and active filtering. This paper presents theoretical, numerical, and experimental analysis of mechanical vibrations in a rectangular ribbon loudspeaker. Several vibration modes of a specific loudspeaker ribbon are simulated and visualized using MATLAB® and COMSOL Multiphysics. Finite Element Method (FEM) modeling is applied, following approaches similar to those reported in [5]. Experimental validation is conducted using video recordings of ribbon vibration modes at 60 frames per second.

2. Theoretical background

2.1. The basic plate theory

The acoustic mass and impedance of ribbon loudspeakers depend on excitation frequency [6], resulting in resonances at different frequencies. These resonant frequencies are influenced by ribbon thickness, material properties, and boundary conditions.

The ribbon loudspeaker strip can be modeled as a thin plate, defined as a solid body bounded by two parallel surfaces whose lateral dimensions are significantly larger than thickness [7,8]. When the ratio of thickness to lateral dimension is less than 1/20, the structure is considered a thin plate [9].

Several mathematical approaches exist for analyzing plate vibrations. Classical plate theory includes Poisson's formulation, Kirchhoff–Love theory, and Mindlin plate theory. Additional methods such as Rayleigh–Ritz, finite strip, and eigenfunction approaches allow analysis under various boundary conditions [10–12].

In this study, the Rayleigh method is used to determine the first natural frequency. Results are compared with FEM simulations and experimental observations.

There are also other approaches for analyzing thin plate vibrations, like the Bessel function method, where various Bessel functions represent the different mechanical vibrations (modes) with different boundary conditions [12]. The first of the strip's modes has the highest amplitude, while the actual deformations of the other modes are significantly smaller [9].

Therefore, the deformation of the strip in the first eigenfrequency (first mode) will

be of most significant research interest in terms of both – the mechanical bending of the strip and the degree of deterioration of the reproduced sound.

In the current paper, the Rayleigh Method has been used to determine the first eigen-frequency of the ribbon loudspeaker. The obtained result has been compared to results from simulations conducted by software products using the Basic Plates Theory for calculating the resonant frequencies. It also has been compared to the 60-fps video recording of the plate mechanical vibrations.

In Basic Plates Theory, some intensities and moments pertain to a unit length of the cross-section [13, 14]. Those are:

- shear forces - Q_x and Q_y;
- bending moments - M_x and Q_y ;
- twisting moments - $M_{xy} = M_{yx}$.

In Fig. 1, the latter are shown, including tangential stresses (σ_x, σ_{xy},σ_{xz}, σ_y, σ_{yx} and σ_{yz}) on the surface of the plate.

The numerical values of the intensities and moments on the plate surface are [13, 14]:

$$Q_x = \int_{-\frac{h}{2}}^{\frac{h}{2}} \sigma_{xz} dz, Q_y = \int_{-\frac{h}{2}}^{\frac{h}{2}} \sigma_{yz} dz, \tag{1}$$

$$M_x = \int_{-\frac{h}{2}}^{\frac{h}{2}} z\sigma_y dz, M_y = \int_{-\frac{h}{2}}^{\frac{h}{2}} z\sigma_x dz, \tag{2}$$

$$M_{xy} = M_{yx} = \int_{-\frac{h}{2}}^{\frac{h}{2}} z\sigma_{xy} dz, \tag{3}$$

where h is the plate thickness.

Due to the plane-strained state of the plate, the tangential stresses σ_z, σ_{zx} and σ_{zy}, will be considerably smaller than σ_x, σ_y, and σ_{xy}, therefore they are neglected. The tangential stresses are known from Hook's law for the two-dimensional strained state [14]:

$$\sigma_x = \frac{E}{1-\upsilon^2} \left(\varepsilon_x + \upsilon\varepsilon_y\right), \tag{4}$$

$$\sigma_y = \frac{E}{1-\upsilon^2} \left(\varepsilon_y + \upsilon\varepsilon_x\right), \tag{5}$$

$$\sigma_{xy} = \frac{E}{2\left(1+\upsilon\right)} \varepsilon_{xy}, \tag{6}$$

where υ is Poisson's ratio, characterizing the elastic properties of the material; E-Young's modulus.

In Eq. (4)-(6) ε_x, ε_y and ε_{xy} are the correlations between the movements and the deformations. Those strain-displacement relations that result in the elastic body being strained due to the applied load are well known from Cauchy's work:

$$\varepsilon_x = \frac{du}{dx'}, \tag{7}$$

$$\varepsilon_y = \frac{d\nu}{dy'}, \tag{8}$$

$$\varepsilon_{xy} = \frac{du}{dy} + \frac{d\nu}{dx'}, \tag{9}$$

where u and ν represent the horizontal movements, subsequently on the X and Y axis, of that point on the plate's surface.

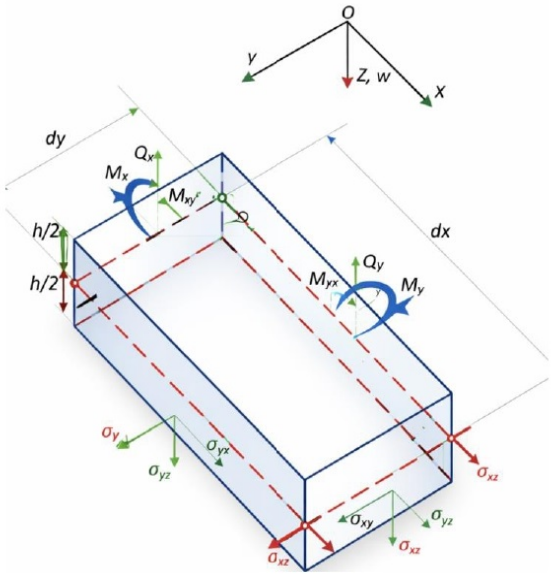

Figure 1: Shear forces, bending and twisting moments and tangential stresses.

After applying Eq. (7)-(9) in Eq. (4)-(6) and then Eq. (4)-(6) in Eq. (1)-(3) and afterward integrating to the plate's thickness (on Z) one obtains:

$$M_x = -D\left(\frac{d^2w}{dx^2} + \upsilon\frac{d^2w}{dy^2}\right), \tag{10}$$

$$M_y = -D\left(\frac{d^2w}{dy^2} + \upsilon\frac{d^2w}{dx^2}\right), \tag{11}$$

$$M_{xy} = -D\,(1-\upsilon)\,\frac{d^2w}{dxdy'}, \tag{12}$$

where $w(x,y)$ is a displacement function; $D = \frac{Eh^3}{12(1-\upsilon^2)}$ – plate stiffness (flexural rigidity of the plate material).

The internal forces and moments can be related when considering equilibrium of the plate elements. Thus, for equilibrium in the X direction, in the absence of body forces [7]:

$$\frac{d\sigma_x}{dx} + \frac{d\sigma_{xy}}{dy} + \frac{d\sigma_{xz}}{dz} = 0. \tag{13}$$

After multiplying Eq. (13) by z and integrating over the thickness of the plate one can assume that:

$$Q_x = \frac{dM_x}{dx} + \frac{dM_{xy}}{dy}. \tag{14}$$

Similarly, one can integrate the equation of equilibrium in the Y direction:

$$Q_y = \frac{dM_y}{dy} + \frac{dM_{xy}}{dx}. \tag{15}$$

Considering the integration over the thickness of the last equilibrium equations in the Z direction one obtains:

$$\frac{d\sigma_{xz}}{dx} + \frac{d\sigma_{yz}}{dy} + \frac{d\sigma_{zz}}{dz} = 0, \tag{16}$$

Integrating the equation of equilibrium in the Z direction, one obtains:

$$\frac{dQ_x}{dx} + \frac{dQ_y}{dy} + q(x,y) = 0, \tag{17}$$

where $q(x,y)$ is a normal load distribution on the top face of the plate.

After replacing Equations (10)-(12), (15) and (16) in Eq. (17) one obtains the nonhomogeneous biharmonic equation of Sophie-Germaine for a plate with constant thickness:

$$\frac{d^4w}{dx^4} + 2\frac{d^4w}{dx^2dy^2} + \frac{d^4w}{dy^4} + \frac{q}{D} = 0. \tag{18}$$

Equation (18) is also known as equation of motion or Euler-Lagrange equation and is usually written as:

$$\nabla^4 w = \frac{q}{D}, \tag{19}$$

where $\nabla^4 = \nabla^2 \cdot \nabla^2$ is the biharmonic operator (∇^2- Laplacian operator).

When the displacement function $w(x,y)$ is known, the deformation form (mode shape) can be represented. This function can be calculated after integrating the equation

of motion Eq. (18) for specific boundary conditions. The roots of the equation will then be resonant (natural) frequencies.

The current article deals with a ribbon loudspeaker whose plate edges are fixed-free-fixed-free, as illustrated in Fig. 2.

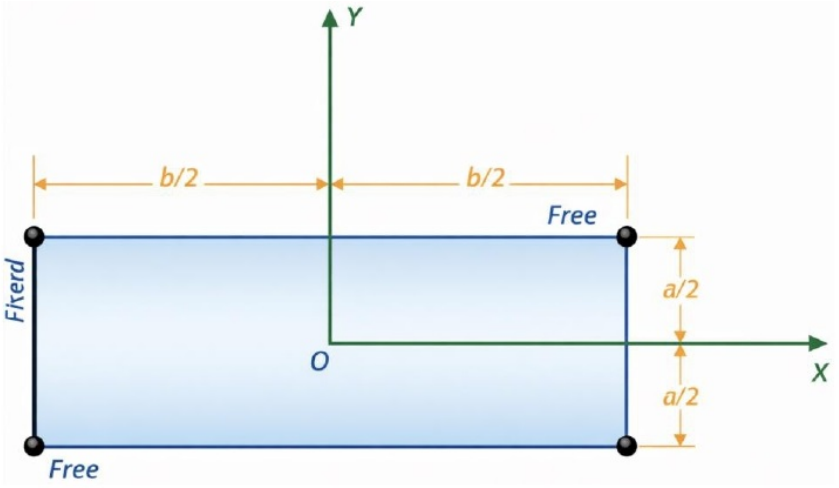

Figure 2. The boundary conditions of the plate edges.

The boundary conditions for calculating the displacement function after integrating the equation of motion for the case at hand (Fig. 2) are [7]:

$$w\left(-b/2,y\right)=0, \tag{20}$$

$$w(+b/2,y)=0, \tag{21}$$

$$\frac{dw}{dx}=0,\ \text{for}\ \left(\pm b/2,y\right). \tag{22}$$

For fixed-free edges. Fixed edge: $w=0$, $\frac{\partial w}{\partial n}=0$. Free edge: $M=0$, $Q=0$. Then, the bending moment M_y and the shear force Q_y on the Y axis are:

$$M_y=-D\left(\frac{d^2w}{dy^2}+\upsilon\frac{d^2w}{dx^2}\right)=0;\ for\ \left(x,\pm\frac{a}{2}\right), \tag{23}$$

$$Q_y=D\frac{d}{dy}\left[\nabla^2w\right]=-D\frac{d}{dy}\left\{\left[\frac{d^2}{dx^2}+\frac{d^2}{dy^2}\right]w\right\}=0. \tag{24}$$

Considering the given boundary conditions, $q = \rho h \frac{d^2w}{dt^2}$ and if one replaces $w(x, y, t) = W(x, y)e^{j\omega t}$ in Eq. (18), the biharmonic equation of a plate with constant thickness will be [14]:

$$\frac{d^4W}{dx^4} + 2\frac{d^4W}{dx^2dy^2} + \frac{d^4W}{dy^4} + \rho h\frac{\omega^2 W}{D} = 0, \tag{25}$$

where ω is angular frequency; ρ - density of the material.

Due to a certain degree of difficulty when solving differential equations of that order, approximate methods for calculating the resonant frequencies and representing the mode shape are used.

The first mode typically dominates structural response under low-frequency excitation; however, the amplitude is not necessarily the highest, as it depends on excitation characteristics, damping, and boundary conditions.

2.2. The Rayleigh method for plates

In the Rayleigh Method, the displacement function is represented by two equations – for strain energy and kinetic energy. With this method, only the upper limit of the fundamental frequency for the first mode can be calculated.

The Rayleigh method provides an upper bound estimate of the fundamental natural frequency when the assumed displacement function satisfies the geometric boundary conditions.

The total kinetic energy of a freely vibrating plate with natural frequency $\omega = \omega_1$ is [7]:

$$T = \frac{1}{2}\int_{-b/2}^{b/2}\int_{-a/2}^{a/2} \rho h \dot{w}(x, y, t)dxdy. \tag{26}$$

A solution of the form is assumed as $w(x, y, t) = W(x, y)e^{j\omega t}$ and thus Eq. (26) can be rewritten:

$$T = \frac{\omega^2}{2}\int_{-b/2}^{b/2}\int_{-a/2}^{a/2} \rho h W_1^2(x, y)dxdy. \tag{27}$$

Eq. (27) will have maximum value when $sin^2\omega_1 t = 1$.

The maximum total strain energy V_{max} of the plate is [7]:

$$V_{max}\frac{D}{2}\int_{-\frac{b}{2}}^{\frac{b}{2}}\int_{-\frac{a}{2}}^{\frac{a}{2}} (\nabla^2 W_1)^2 dxdy, \tag{28}$$

$$\frac{D}{2}\int_{-b/2}^{b/2}\int_{-a/2}^{a/2}\left[2(1-\upsilon)\left\{\left(\frac{d^2W_1}{dxdy}\right)^2 - \frac{d^4W_1}{dx^2dy^2}\right\}\right]dxdy. \tag{29}$$

For a conservative system by Rayleigh's principle [15] one can equalize the maximum kinetic energy Eq. (27) and maximum strain energy Eq. (28) of the system and extract the natural frequency $\omega = \omega_1$, so:

$$\omega_1^2 = \frac{D\int_{-b/2}^{b/2}\int_{-a/2}^{a/2}\left[(\nabla^2 W_1)^2 + 2(1-\upsilon)\left\{W_{1,xy}^2 - W_{1,xx}W_{1,yy}\right\}\right]dxdy}{\rho h\int_{-b/2}^{b/2}\int_{-a/2}^{a/2} W_1^2 dxdy}, \quad (30)$$

where $W_{1,xy} = \frac{d^2W_1}{dxdy};;W_{1,xx} = \frac{d^2W_1}{dx^2}\ and\ W_{1,yy} = \frac{d^2W_1}{dy^2}$, are Rayleigh's Quotient and give the fundamental natural frequency of the plate.

The Rayleigh method's accuracy can be improved using the Rayleigh–Ritz method or other more sophisticated methods to calculate all resonant frequencies.

3. Numerical modeling and simulation

3.1. Finite Element Model Description

The structural behaviour of the system was investigated using a finite element modeling (FEM) approach. The geometry was defined based on the actual physical configuration of the specimen, with particular attention given to thickness, material properties, and boundary conditions.

Due to the extremely small thickness of the structure, shell (or thin solid) elements were employed to accurately capture bending behaviour. The material was assumed to be homogeneous and isotropic, with linear elastic properties.

Boundary conditions were defined to represent quasi-free constraints, consistent with the experimental setup. This choice is critical, as it directly influences the resulting natural frequencies and mode shapes.

3.2. Numerical implementation (MATLAB)

A complementary numerical model was developed in MATLAB to support analytical evaluation and validation of the FEM results. The governing dynamic equation of motion was formulated in matrix form as:

$$M\ddot{u} + Ku = 0, \quad (31)$$

where M and K represent the mass and stiffness matrices, respectively.

The eigenvalue problem was solved to obtain natural frequencies and corresponding mode shapes. Numerical routines were implemented to ensure stability and consistency of the solution, enabling comparison with FEM-based results.

3.3. COMSOL Multiphysics simulation

The finite element simulations were performed using COMSOL Multiphysics, which provides a robust environment for Multiphysics analysis. A frequency domain and eigenfrequency analysis were conducted to identify the natural frequencies and deformation modes of the structure. Mesh sensitivity analysis was performed to ensure numerical convergence and reliability of the results.

The simulation results revealed a dominant response in the low-frequency range, with a significant displacement peak observed around 24 *Hz*. This behaviour is consistent with the reduced structural stiffness associated with the thin geometry and quasi-free boundary conditions.

3.3.1. Model Validation

The numerical results were validated against experimental observations. A pronounced displacement response was recorded in the frequency range around 24 *Hz*, showing good agreement with the predicted natural frequency.

This validation confirms that the developed numerical model adequately captures the essential dynamic characteristics of the system and can be reliably used for further analysis.

3.4. Experimental setup and results

Matlab® and COMSOL Multiphysics were used to calculate the resonant frequencies and to simulate the corresponding mode shapes on the surface of the plate. Both software products use Basic Plate Theory for the calculations.

Frequency generator, Power Amplifier, Ribbon Loudspeaker-VLD 40, DAQ System, Digital Multimeter and a High-speed Camera (60 fps) are used for video recording of the modes (the experimental setup is shown in Fig. 3). The properties of the loudspeaker's plate are given in Table 1.

The ribbon thickness of 14 μm is typical for aluminum ribbon loudspeakers and ensures low mass and high responsiveness.

For better understanding and accuracy of the comparative analysis the author demonstrates one more method for calculating the first natural frequency - the Rayleigh Method. (A Matlab§based software program is used [16]. The calculations point that the natural frequency of a plate in the case study is 24 *Hz*.

The low natural frequency can be explained by the combination of extremely small thickness, low bending stiffness, and quasi-free boundary conditions, all of which significantly reduce the global structural rigidity.

Importantly, this behaviour is experimentally validated, as a pronounced displacement peak was observed around 24 *Hz* in the test setup, in close agreement with the

numerical model.

In Table 2 resonant frequencies and corresponding distortion, the resonant frequencies and their corresponding mode shapes are represented. Those are calculated using Matlab® and COMSOL Multiphysics products which uses FEM to implement the Basic Plate Theory.

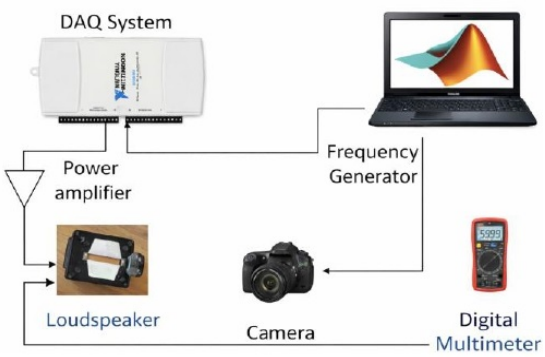

Figure 3. Experimental setup diagram.

Table 1. Plate properties

Young's Modulus, *GPa*	70
Poisson's Ratio	0,33
Mass Density, kg/m^3	2700
Thickness, *mm*	0,014
Width, *mm*	8,6
Length, *mm*	56
Material	Aluminum

The video recording, where some of the calculated modes are visible, is available in [20]. A careful review of the video recording reveals detectable distortions in the plate. The most pronounced deformation is observed in the first mode at 24 *Hz*. Additionally, higher order modes such as the 7th mode at 312 *Hz* are also discernible. Theoretical analysis, as depicted in Table 2, reveals that as the frequency rises, the deformations of the surface of the plate become more complex. The complex combination of shear forces, bending and twisting moments and the fixed position of the short edges of the plate lead to various deformations on its surface.

The experimental setup provides qualitative validation of the observed behaviour. The excitation frequency was monitored using a UT70 series digital multimeter, providing sufficiently reliable values for identifying resonance effects.

Table 2 presents the calculated natural frequencies along with the corresponding mode shapes obtained from both MATLAB-based analytical modeling and COMSOL Multiphysics simulations. The 2D representations illustrate the displacement distribution, while the 3D visualizations provide a spatial interpretation of the deformation patterns.

In this case, the analysis refers to a specific structural configuration and excitation scenario. The first mode governs the global structural response of the system. However, structural damage is primarily driven by the magnitude of physical displacement rather than the modal order. The experimentally observed large-amplitude deformation around 24 Hz indicates that the dominant risk is associated with displacement levels, while higher-order modes mainly contribute to localized deformation and acoustic distortion.

Accuracy depends on mesh density, element type, and convergence analysis. A mesh convergence study should be performed to validate numerical precision.

Table 2. Calculated resonant frequencies and corresponding distortion

№	Frequence, *Hz*	Matlab (3D)	Matlab (2D)	COMSOL (3D)	COMSOL (2D)
1	Matlab – 23.38 COMSOL –23.87	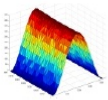		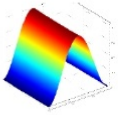	
2	Matlab – 64.51 COMSOL – 65.77	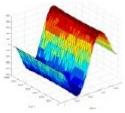	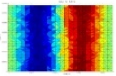	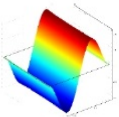	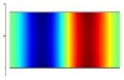
3	Matlab – 96.86 COMSOL – 98.90	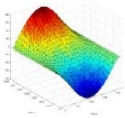	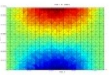	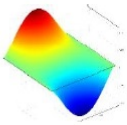	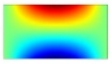
4	Matlab – 126.60 COMSOL – 129.17	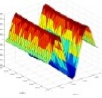	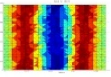	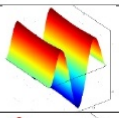	
5	Matlab – 197.70 COMSOL – 201.93	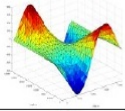	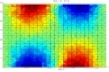	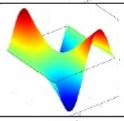	
6	Matlab – 210.10 COMSOL – 214.13	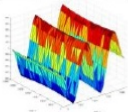	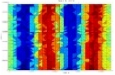	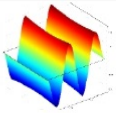	
7	Matlab – 306.00 COMSOL – 312.86	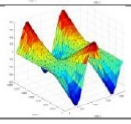		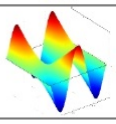	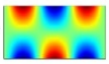
8	Matlab – 314.80 COMSOL – 320.88	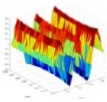		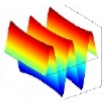	

Below is a scientific analysis of the presented Table 2 with calculated resonant frequencies and deformation modes obtained in Matlab and COMSOL in 2D and 3D settings. Comparison of resonant frequencies (Matlab vs COMSOL) is shown in Table 3.

Table 3. Comparison of resonant frequencies (Matlab vs COMSOL)

Mode No.	Matlab (*Hz*)	COMSOL (*Hz*)	Deviation
1	23,38	23,87	˜ +2,1%
2	64,51	65,77	˜ +2,0%
3	96,86	98,90	˜ +2,1%
4	126,60	129,17	˜ +2,0%
5	197,70	201,93	˜ +2,1%
6	210,10	214,13	˜ +1,9%
7	306,00	312,86	˜ +2,2%
8	314,80	320,88	˜ +1,9%

The discrepancy is within 1,9–2,2%, which is normal for comparison between the analytical (Rayleigh/plate theory) and FEM models.

The experimental validation is qualitative, based on visual observation of vibration modes using high-speed video. Due to equipment limitations, precise frequency measurement and uncertainty estimation were not performed.

4. Results and discussion

Table 2 presents the calculated resonant frequencies and the corresponding deformation modes of the investigated plate, obtained using Matlab and COMSOL Multiphysics in both two-dimensional (2D) and three-dimensional (3D) formulations. The comparison is performed for the first eight natural vibration modes in order to validate the analytical–numerical model and to assess the accuracy of the finite element approach.

As shown in Table 2, the resonant frequencies calculated using COMSOL are consistently higher than those obtained from the Matlab model for all considered modes. The observed discrepancy between the two methods remains within the range of approximately 1,9–2,2%, which is acceptable for mechanical vibration problems involving analytical approximations and finite element discretization.

This systematic difference can be attributed to the simplified assumptions adopted in the Matlab model, such as idealized boundary conditions and reduced dimensionality, whereas the COMSOL model employs a full three-dimensional finite element formulation. The latter allows for a more accurate representation of the plate geometry, stiffness distribution, and mass effects, resulting in slightly higher predicted eigenfrequencies. Consequently, the COMSOL results may be regarded as more representative of the actual physical behavior of the structure.

Despite the minor numerical differences in resonant frequencies, the deformation patterns obtained from Matlab and COMSOL exhibit a high degree of qualitative agreement. For each vibration mode, the spatial distribution of displacement, the number

of nodal lines, and the symmetry properties are identical across both software environments. This confirms the correctness of the modal identification and indicates that both models describe the same physical vibration phenomena.

The first and second modes are characterized by simple bending shapes with one or two dominant antinodes, corresponding to the fundamental flexural behavior of the plate. Higher-order modes exhibit increasingly complex deformation patterns, including multiple nodal lines and localized regions of maximum displacement. Such complexity becomes particularly evident for modes above 200 *Hz*, where the plate response shows strong spatial variation.

The comparison between 2D and 3D visualizations further supports the consistency of the results. The 2D representations provide a clear illustration of the displacement amplitude distribution and nodal regions, while the 3D plots offer a more intuitive depiction of the actual mechanical deformation of the structure. In both Matlab and COMSOL, the 2D and 3D mode shapes are mutually consistent, confirming that the reduced-dimensional visualization does not distort the underlying physical behavior.

From an engineering perspective, the first resonant mode, occurring at approximately 23–24 *Hz*, is of particular importance, as it may significantly affect the structural integrity of the plate (or loudspeaker strip) under operational excitation. Higher-order modes in the range of 200–320 *Hz* may induce localized stresses and contribute to mechanical fatigue or acoustic distortion, especially under prolonged dynamic loading.

The results presented in Table 2 demonstrate strong agreement between the Matlab and COMSOL models in terms of modal shapes and acceptable agreement in resonant frequencies. The slight frequency overestimation observed in the COMSOL results is consistent with the higher fidelity of the finite element method. Overall, the comparison validates the analytical–numerical approach and confirms the reliability of the finite element model for further parametric and optimization studies.

5. Conclusion

The results presented in Table 2, together with the fundamental frequency calculated using the Rayleigh Method [16-19], confirm the validity of the underlying theoretical assumptions. The Eigen frequency corresponding to the first vibration mode, obtained via the Rayleigh Method, is higher than the fundamental frequency predicted by Basic Plate Theory. This discrepancy is significant, as it may influence the structural integrity of the plate, particularly the ribbon (strip) element of the loudspeaker, where excessive vibration amplitudes can lead to mechanical degradation or failure.

The Matlab® implementation of the Rayleigh Method [16] computes only the first mode of vibration, which is characterized by the largest displacement amplitude. However, this approach does not emphasize high accuracy nor does it provide higher-order Eigen frequencies. In contrast, Basic Plate Theory offers a more comprehensive and

accurate framework, allowing the calculation of multiple Eigen frequencies and corresponding mode shapes, thereby providing a more complete description of the dynamic behavior of the plate.

The minor discrepancies observed between the Eigen frequencies obtained using Matlab® and COMSOL Multiphysics can be attributed primarily to the different numbers of finite elements employed in the numerical models-6656 elements in COMSOL Multiphysics versus 576 elements in Matlab® . This variation in mesh density directly affects numerical precision, particularly for higher modes.

Experimental observations further support the numerical findings. As demonstrated in the video recording [20], a pronounced plate displacement corresponding to the first vibration mode is observed at approximately 24 *Hz*. This experimentally detected resonance aligns closely with the results obtained from both the Rayleigh Method and Basic Plate Theory, thereby validating the numerical analysis. Nevertheless, due to inherent limitations of the recording equipment, the majority of higher-order vibration modes could not be clearly resolved.

Overall, the combination of numerical simulations, mode shape analysis, and experimental visualization significantly enhances the theoretical understanding of the vibrational behavior of ribbon-type loudspeaker elements. The results of this study are therefore directly applicable to the design optimization and manufacturing of ribbon loudspeakers, particularly in mitigating undesirable resonances and improving acoustic performance.

The Rayleigh method provides an approximate estimate of the fundamental frequency, and differences with FEM results depend on assumed mode shapes and modeling assumptions.

ACKNOWLEDGEMENTS The authors acknowledge funding from the Ministry of Education and Science of the Republic of Bulgaria under the National Science Program “Security and Defense”, in implementation of the Decision of the Council of Ministers of the Republic of Bulgaria No: 731/21.10.2021 and according to Agreement No: D01-74/19.05.2022.

References

[1] Liyang G., Li T., Meiying H., Yilong, H. (2022) Distributed Two modes of motions for a single disk on the vibration stage. J. Phys.: Condens. Matter., 36(11), 115102.

[2] Liyang G., Li T., Meiying H., Yilong, H. (2021) Dynamics of a vibration-driven single disk. Scientific Reports, 11(1), 16561.

[3] Klippel W. (2009) Distributed Mechanical Parameters Describing Vibration and Sound Radiation of Loudspeaker Drive Units. International Symposium on ElectroAcoustic Technologies, 1-19.

[4] Duan W., Wang C., Wang C. (2008) Modification of fundamental vibration modes of circular plates with free edges. Journal of Sound and Vibration, 709-715.

[5] Vanam B., Rajyalakshmi M., Inala R. (2012) Static analysis of an isotropic rectangular plate using finite element analysis (FEA). Journal of Mechanical Engineering Research, 4 (4), 2148-162.

[6] Beranek L., Mellow J. (2019) Acoustics: Sound Fields and Transducer. Academic Press, 871 p.

[7] Chakraverty S. (2009) Vibration of Plates., CRC Press, 411 p.

[8] Chakraverty S. (2016). Vibration of Functionally Graded Beams and Plates. Academic Press, 241 p.

[9] Dada M., Popoola P., Mathe N., Adeosun S., Aramide O. (2022) 2D numerical model for heat transfer on a laser deposited high entropy alloy baseplate using Comsol Multiphysics. Materials Today: Proceedings, 50(5), 2541-2546.

[10] Xing Y., Liu B. (2009) Closed form solutions for free vibrations of rectangular Midlin plates. Acta Mechanica Sinica, 25, 689-698.

[11] Hashemi S.S., Arsanjani M. (2005) Exact characteristic equations for some of classical boundary conditions of vibrating moderately thick rectangular plates. International Journal of Solids and Structures, 42, 819-853.

[12] Wu J., Liu A., Chen H. (2024) Exact Solutions for Free-Vibration Analysis of Rectangular Plates Using Bessel Functions. Journal of Applied Mechanics, 74, 1247-1251.

[13] Muhammad M.A., Yubin C., Izaz R., Salman K., Heung S.K. (2025) Intelligent Computational Methods for Damage Detection of Laminated Composite Structures for Mobility Applications: A Comprehensive Review. Archives of Computational Methods in Engineering, 32, 441-469.

[14] Zhen Z.,Yinglong Z., Yinglong Z., Feng C. (2025) A Review of Vibration Control Studies of Double-Layered Cylindrical Shells Under Transient Excitation in Water. J. Mar. Sci. Eng., 13(7), 1238.

[15] Lukasz S., Davide A., Francesco C. (2025) Advances in Noise and Vibrations for Machines. Machines, 13(8), 723.

[16] Hong H.L., Van K.T., Nhan T.H., Nguyen N.M.H. (2025) The impacts of variable nonlocal, length-scale factors and surface energy on hygro-thermo-mechanical

vibration and buckling behaviors of viscoelastic FGP nanosheet on viscoelastic medium. Acta Mechanica Sinica, 41, 124135.

[17] Islamov I.J. (2023) Modeling the Attenuation of a Microwave Signal, Taking Into Account the Specific Features of the Terrain for Unmanned Aerial Vehicles. International Journal of Microwave and Optical Technology, 18(2), 131-139.

[18] Islamov I., Bashirov R., Ismayilov N. (2023) Modeling of a Telecommunication Optical Waveguide with Anisotropic Medium. International Journal of Microwave and Optical Technology, 18(5), 540-549.

[19] Islamov I.J., Agayev F.G., Aliyeva G.V. (2025) Electrodynamic Modeling of a Planar Antenna System for Wireless Communicatıon. Advanced Physical Research, 7(1), 87-101.

[20] Iliev I. (2024) Vibrations of Thin Rectangular Plates. Mendeley Data, 1, 1-8.

Islam J. Islamov
Baku Engineering University, Baku, Azerbaijan
E-mail: isislamov@beu.edu.az

Kalin S. Kalinov
Nikola Vaptsarov Naval Academy, Varna, Bulgaria
E-mail: info@naval-acad.bg

Iliyan Y. Iliev
Nikola Vaptsarov Naval Academy, Varna, Bulgaria
E-mail: i.y.iliev@naval-acad.bg

Received 10 December 2025
Accepted 08 April 2026